A Modified Four-State Model for the "Dual Fluorescence" of N^6,N^6-Dimethyladenine Derived from Femtosecond Fluorescence Spectroscopy†

Nina K. Schwalb* and Friedrich Temps*,†

Institut für Physikalische Chemie, Christian-Albrechts-Universität zu Kiel, Olshausenstrasse 40, D-24098 Kiel, Germany

Received: March 11, 2009; Revised Manuscript Received: May 12, 2009

The radiationless deactivation of the excited electronic states of the dual fluorescence molecule N^6,N^6-dimethyladenine (DMAde) was investigated using femtosecond time-resolved fluorescence up-conversion spectroscopy. The molecules were studied in solution in water and in dioxane. Fluorescence−time profiles were recorded in the wide wavelength range of $290 \leq \lambda_{fl} \leq 650$ nm. The excitation wavelengths in the region of the first UV absorption band were tuned from close to the electronic origin ($\lambda_{pump} = 294$ nm) to excess energies of ~5400 cm^{-1} above ($\lambda_{pump} = 258$ nm). Global fits to the measured curves turned out to reflect distinctive molecular relaxation processes on five well-defined time scales. Sub-100 fs and 0.52(3) ps lifetimes were found to predominate at the shortest UV and blue emission wavelengths in water, 1.5(1) and 3.0(2) ps components at intermediate wavelengths and a 62(1) ps value in the red region of the spectrum (2σ error limits of the last digits in parentheses). In dioxane, these lifetimes changed to ≤0.27 and 0.63(4) ps in the UV, 1.5(1) and 10.9(10) ps in a wide range of intermediate, and 1.40(4) ns at the longest wavelengths. However, little dependence of the respective time constants on λ_{pump} was observed, indicating that the ensuing relaxation processes proceed via practically barrierless pathways through conical intersections. Building on the knowledge for the parent molecule adenine (Ade), the observations were rationalized with the help of a modified four-state model for the electronic dynamics in DMAde with the $\pi\pi^*(L_a)$, $\pi\pi^*(L_b)$, and $n\pi^*$ states similar to those in Ade and an intramolecular charge-transfer (ICT) state, which has no counterpart in Ade, responsible for the long-wavelength fluorescence.

1. Introduction

The DNA bases stand out for very low fluorescence quantum yields ($\Phi \leq 10^{-4}$), owing to ultrafast nonradiative electronic deactivation processes, which rapidly return the energized molecules to their electronic ground states before chemical reactions in the excited states can cause profound molecular damage.[1] The underlying photophysical and photochemical mechanisms are of crucial importance for protecting the genomic information encoded in the DNA against UV photodamage and have thus attracted ubiquitous attention for years.

The purine base adenine (Ade) has arguably been studied in most detail. Within the last years, femtosecond transient absorption and fluorescence up-conversion measurements in aqueous solution have provided excited-state lifetimes for the canonical 9H-Ade ($\tau \approx 0.3$ ps) and for the minor 7H-Ade tautomer ($\tau \approx 8$ ps) that coexists in equilibrium with the 9H form.[2−9] The time-resolved investigations have been complemented by studies of vibronically resolved spectra,[10−16] experiments on H-atom loss dynamics,[17−20] and temporally resolved multiphoton ionization[21−24] and photoelectron measurements[25−27] of supersonically cooled Ade in molecular beams. Furthermore, theoretical investigations[28−38] pointed out several possible nonradiative electronic deactivation pathways through conical intersections (CIs) between the nearly isoenergetic $\pi\pi^*$, $n\pi^*$, and $\pi\sigma^*$ electronic states in the region of the first UV absorption band and the S_0 ground state. A consensus appears to have emerged that the short lifetime of the optically bright excited $\pi\pi^*(^1L_a)$ state in 9H-Ade arises due to a very fast barrierless internal conversion pathway through a CI to the S_0 state involving a large-amplitude puckering motion of the C^2H group of the six-membered ring.

SCHEME 1

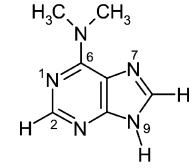

A striking feature of the purine bases is that very small modifications to the structure of the chromophore can strongly alter the electronic dynamics. An important example is 2-aminopurine (2AP), a highly fluorescent structural isomer of Ade (≡ 6-aminopurine) that is widely used as a fluorescence marker in DNA.[39−43] However, the arguably most eye-catching (and in comparison to Ade or 2AP, not at all well-understood) case is that of N^6,N^6-dimethyladenine (DMAde, Scheme 1), a molecule that is known to emit so-called dual fluorescence.[44−46]

DMAde exists in solution at room temperature virtually only in its 9H tautomeric form because of the higher steric demands of the dimethylamino compared to those of the amino group of Ade.[44−46] Its strong $\pi\pi^*$ UV absorption is very similar to that of Ade, but while the fluorescence of Ade is in the near-UV and shows only a small, normal Stokes shift,[6] DMAde exhibits two widely separated emission bands. The so-called B band, which peaks in the near-UV at $\lambda_{fl} \approx 330$ nm, resembles the

† Part of the "Robert W. Field Festschrift".

* To whom correspondence should be addressed. E-mail: schwalb@phc.uni-kiel.de.

† E-mail: temps@phc.uni-kiel.de.

10.1021/jp9021773 CCC: $40.75
Published on Web 07/01/2009

emission from Ade and is thus attributed to the local excited (LE) state associated with the purine chromophore. In contrast to Ade, however, the main fluorescence of DMAde is observed in the visible spectral region, peaking at between $\lambda_{fl} \approx 450$ and 550 nm depending on the solvent. The emission in this so-called A band strongly predominates in nonpolar aprotic solvents, but the red shift is most pronounced in more polar solvents. Resembling the prototypical case of dimethylaminobenzonitrile (DMABN),[47] the dual fluorescence of DMAde has been explained in the literature by a transformation from the LE state to an intramolecular charge-transfer (ICT) state involving the dimethylamino group and the purine ring as the electron donor and acceptor, respectively.[44−46]

Recently, we reported on a femtosecond time-resolved fluorescence up-conversion study of the excited-state lifetimes of DMAde in water.[48] Measurements were performed using an electronic excitation wavelength of $\lambda_{pump} = 258$ nm at a series of emission wavelengths ranging over $320 \leq \lambda_{fl} \leq 650$ nm. We found that the fluorescence−time profiles in the UV were dominated by a short-lived decay component with a subpicosecond lifetime ($0.2 \leq \tau \leq 0.6$ ps), whereas the time profiles in the visible were represented in essence by a long-lived component ($\tau \approx 60$ ps). The results could be interpreted using a modified ICT model assuming a reversible excited-state reaction to account for weak long-lived fluorescence components in the UV range, which could not be explained by former models. Additionally, a fast direct nonradiative deactivation pathway from the LE to the S_0 state and vibrational cooling/relaxation processes were taken into account.[48] Nevertheless, we pointed out that, in view of the observed ultrafast time scales, simple kinetic models might not hold for DMAde and that specific wavepacket motions through CIs between the excited-state potential energy hypersurfaces (PEHS) should be considered as in the case of Ade. Moreover, since both molecules have the same chromophore, any photophysical model for the dual fluorescence of DMAde should build upon the available information on the excited electronic state structure and dynamics for the parent molecule Ade.[28−38] Indeed, Canuel et al.[23] studied electronically excited DMAde in a supersonic jet experiment and observed fast nonradiative deactivation dynamics comparable to that of Ade under similar conditions, but they did not allude further to the dual fluorescence problem since solvation is usually considered a requirement for ICT. Last but not least, we previously used excitation pulses at a relatively short, fixed wavelength, $\lambda_{pump} = 258$ nm, which prepared the DMAde molecules with a substantial amount of excess energy above the origin of their excited electronic state. Further work was deemed to be necessary to elucidate the electronic dynamics at energies in the region close to the supposed threshold for the ICT reaction.

In this paper, we present the results of a new, more comprehensive time-resolved fluorescence up-conversion study of the excited-state lifetimes of DMAde in two solvents, water and dioxane, to address those issues. Measurements were done at excitation wavelengths in the range of $258 \leq \lambda_{pump} \leq 294$ nm in order to scan the excited-state PEHS down to the electronic origin and elucidate possible potential energy barriers for the excited-state ICT reaction. Fluorescence decays were monitored at numerous detection wavelengths λ_{fl} in the range of $290 \leq \lambda_{fl} \leq 650$ nm. Rise times of the visible emission were investigated by reference to highly fluorescent laser dyes as clocks. The results shed interesting new light on the excited-state relaxation dynamics and the dual fluorescence of DMAde.

2. Experimental Section

2.1. Static Absorption and Fluorescence Spectra. Static absorption and emission spectra were recorded on a Shimadzu 2401 UV desktop and a Horiba Jobin Yvon Fluoromax 4 fluorescence spectrometer, respectively. While the absorption spectra were taken at the same concentration as that used in the time-resolved experiments, the sample concentration was diluted by a factor of ~200 for the static fluorescence measurements to avoid inner filtering effects.

2.2. Fluorescence Up-Conversion Experiments. All time-resolved fluorescence measurements were carried out at room temperature employing a sample cell with a 1 mm optical path length and 0.2 mm fused silica windows. Solutions of DMAde (Sigma-Aldrich, ≥98%) in water (bidest.) or in dry dioxane (Merck Uvasol, ≥99.9%) at concentrations of typically 10^{-3} M were continuously pumped through the cell by a peristaltic pump (Ismatec). UV excitation pulses in the range of $258 \leq \lambda_{pump} \leq 296$ nm were supplied by a home-built frequency-doubled tunable noncollinear optical parametric amplifier (NOPA)[49] providing pulses of <50 fs duration (fwhm) after prism compression. The NOPA was pumped with the second harmonic from a regeneratively amplified Ti:Sa femtosecond laser system (Clark MXR CPA 2001) at $\lambda = 775$ nm with a 1 kHz repetition rate and a ~150 fs (fwhm) pulse duration. The resulting UV excitation pulses (~0.1−0.2 μJ) were separated from the fundamental using dielectric mirrors and focused into the sample cell to a spot size of ~400 μm diameter. The transmitted pump beam was caught by a beam stop, and residual scattered pump light was eliminated by a 1 mm long-pass filter (LOT).

The excited fluorescence was collected and refocused by a pair of off-axis parabolic mirrors (Melles−Griot, $f = 119$ mm) into a 0.1 mm BBO crystal ($\theta = 54.5°$, GWU) for up-conversion by type-I noncollinear sum frequency generation (SFG) with the gate pulses (~100 μJ) at $\lambda = 775$ nm from the Ti:Sa laser. The polarization of the pump beam was rotated to the magic angle with respect to the gate beam to avoid fluorescence depolarization effects. The up-converted light was then focused onto the entrance slit of an $f = 0.1$ m double monochromator (Jobin-Yvon HR 10) and detected with a photomultiplier (Hamamatsu R1527P) connected to a preamplifier (Stanford Research SR 445) and gated photon counter (Stanford Research SR 400). We notice that type-II SFG would normally be the method of choice for fluorescence up-conversion in the visible spectrum, where one could also improve the time resolution,[50] but it cannot be applied at the UV wavelengths of interest here. We therefore opted to stay with type-I SFG for all fluorescence wavelengths to avoid having to exchange the up-conversion crystal during the experiments. Using our setup, we could observe the fluorescence of DMAde in the entire range of emission wavelengths of $290 \leq \lambda_{fl} \leq 650$ nm (up-converted wavelengths over $211 \leq \lambda_{SFG} \leq 354$ nm) just by tilting the SFG crystal by a few degrees without having to realign the optical setup between scans for different λ_{fl}. A small gap remained only around $\lambda_{fl} = 387.5$ nm ($\lambda_{SFG} = 258$ nm) due to interfering third harmonic signals from the intense gate pulses in the up-conversion crystal. The temporal fluorescence decay profiles could be recorded for delay time intervals up to $\Delta t \approx 900$ ps using a 150 mm linear translation stage (Physik Instrumente M-415CG) in the gate beam path.

The instrument response function (IRF) was determined by cross correlation of scattered pump light with the gate pulses. The width of the IRF corresponded to a standard deviation of a Gaussian of $\tau_{IRF} = 0.22 \pm 0.02$ ps, which was the approximate time resolution of our experiments. Time zero values (t_0),

especially for rise time measurements at the red fluorescence wavelengths, were determined by reference to the emission of selected laser dyes with fast fluorescence rise times. Furthermore, within the experimental error limits, test measurements carried out at 10 times higher DMAde concentrations (10^{-2} M) gave identical results.

2.3. Data Analysis. The recorded fluorescence−time profiles were analyzed by nonlinear least-squares fit routines based on the Levenberg−Marquardt algorithm implemented in Mathematica.[51] The different curves were first individually fitted using sums of exponential decay functions with time constants τ_i and amplitudes a_i convoluted with a Gaussian describing the IRF. All parameters were initially allowed to float freely. The IRF widths determined by these fits agreed with the pump−gate cross correlation value given above. Subsequently, a global fitting procedure was applied to the data for each λ_{pump}. Toward these ends, the time zero (t_0) values for all profiles were fixed at the respective values from the individual fits. As it turned out that this analysis returned the same set of decay times for a given λ_{fl} independent of the respective pump wavelength used, an overall global fit was finally carried out on all time profiles (λ_{fl}) at all λ_{pump} for a given solvent. Again, all parameters except the t_0 values were floated. Decay components which received relative amplitudes from the fit of less than one-half of their standard deviation at some particular fluorescence wavelengths λ_{fl} were then successively eliminated from the model until a satisfactory representation of all data curves was reached with minimal numbers of exponentials. The final fit thus provided a set of global time constants and spectral amplitudes (τ_i, a_i) for each fluorescence wavelength λ_{fl}.

Transient emission spectra of the molecules in water and in dioxane were reconstructed from the measured fluorescence decay profiles by normalizing the time-integrated intensities against the intensities of the measured static fluorescence spectra using the approach introduced by Maroncelli and Fleming,[52−54] as already described in our first publication on DMAde in water.[48]

3. Results

3.1. Static Absorption and Fluorescence Spectra. Figure 1a displays the measured static absorption spectra of DMAde in water and in dioxane. Both spectra, normalized for better comparison, are similar and have their maxima at $\lambda = 276$ and 275 nm, respectively. The peak absorption wavelengths are red shifted by about 15 nm compared to the parent molecule Ade, indicative of a stabilization of the excited state(s) by the two methyl groups at the exocyclic amino N atom. In dioxane, the absorption band exhibits a discernible shoulder in its red wing. As for the parent molecule Ade,[55] the main band is assigned to the strong $\pi\pi^*(L_a) \leftarrow S_0$ absorption and the shoulder to the weaker $\pi\pi^*(L_b) \leftarrow S_0$ absorption. The more polar $\pi\pi^*(L_a)$ state is more efficiently stabilized by the solvation in water than the $\pi\pi^*(L_b)$ state.

The static fluorescence spectra of DMAde in the two solvents are depicted in Figure 1b and c, respectively. As mentioned, DMAde clearly exhibits two fluorescence bands, one appearing in the UV (B band) and the red-shifted second one in the visible (A band). Both spectra agree qualitatively and quantitatively with previous reports.[44,45] As shown, they can be nicely fitted by a sum of two log-normal functions. In water, the peak wavelengths are approximately $\lambda_{fl,B} \approx 340$ nm and $\lambda_{fl,A} \approx 530$ nm. Both bands have roughly equal intensities. In contrast, the A band is drastically enhanced in dioxane. In addition, there are solvent-dependent blue shifts of both band maxima in

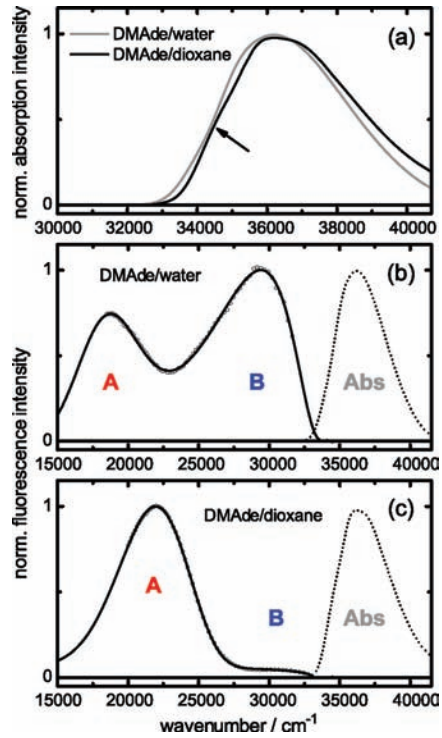

Figure 1. (a) Static absorption spectra of DMAde in water and in dioxane. The arrow marks the shoulder in the spectrum in dioxane. The amplitudes have been normalized for better comparison. (b, c) Normalized static emission spectra (solid lines with small open circles) of DMAde in water and dioxane. The fluorescence bands are labeled B and A for the UV and the visible emission bands, respectively. The symbols represent experimental data, and the lines show fits using a sum of two log-normal functions (one each for the A and B bands). The absorption spectra are given by dotted lines.

dioxane to $\lambda_{fl,B} \approx 330$ nm and $\lambda_{fl,A} \approx 450$ nm. Accepting measurements on the derivatives N^6,N^6-dimethyladenosine and N^6,N^6-dimethyl-9-ethyladenine,[44,45] the fluorescence quantum yields are on the order of $\Phi_{fl,B} \approx 2.8 \times 10^{-4}$ and $\Phi_{fl,A} \approx 2.2 \times 10^{-4}$ in water versus $\Phi_{fl,B} \approx 3.5 \times 10^{-4}$ and $\Phi_{fl,A} \approx 7.1 \times 10^{-3}$ in dioxane.

3.2. Fluorescence−Time Profiles. ***3.2.1. DMAde in Water.*** The temporal fluorescence profiles of DMAde in water were investigated after excitation of the molecules at two wavelengths, $\lambda_{pump} = 258$ and 294 nm.

The previously reported data[48] for $\lambda_{pump} = 258$ nm were complemented by additional measurements in the very blue region of the emission band, at $\lambda_{fl} = 300$ and 310 nm; $\lambda = 300$ nm is the wavelength where the emission and absorption bands of DMAde intersect (cf. Figure 1) and therefore marks the position of the electronic origin. The temporal evolutions in the first 15 ps at the selected emission wavelengths with this pump wavelength are displayed in Figure 2. The progressions of these time profiles toward longer time delays (up to $\Delta t = 450$ ps) were depicted in our earlier publication. As can be seen, the curves at the shortest fluorescence wavelengths exhibit mean decay times of $\langle\tau\rangle < 1$ ps, but those values increase to $\langle\tau\rangle \approx 60$ ps at the most red-shifted wavelengths.

Further time profiles were collected using $\lambda_{pump} = 294$ nm, which excites the DMAde molecules to just above the electronic origin. Owing to the weak absorbance at this pump wavelength, reliable data with satisfactory signal-to-noise ratios could only be determined in the window from $350 \leq \lambda_{fl} \leq 510$ nm. Typical experimental data at four selected fluorescence wavelengths are shown in Figure 3a in comparison with time profiles at similar

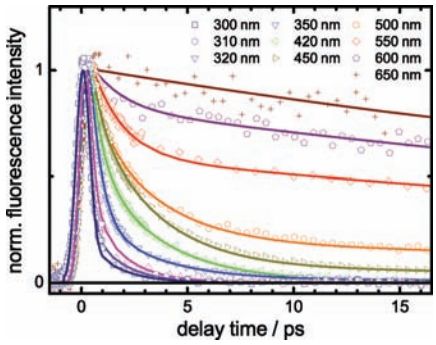

Figure 2. Normalized fluorescence decay profiles of DMAde in water excited at $\lambda_{pump} = 258$ nm at 10 different fluorescence wavelengths in the range of $300 \leq \lambda_{fl} \leq 650$ nm. Open symbols: Experimental data points. Solid lines: Fitted curves from global data analysis (see text).

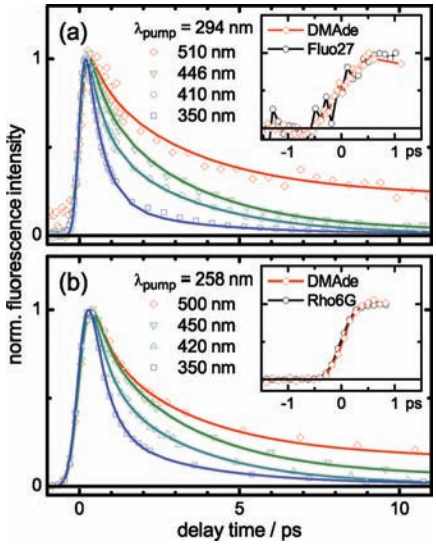

Figure 3. Comparison of the fluorescence decay profiles of DMAde in water excited at (a) $\lambda_{pump} = 294$ nm and (b) $\lambda_{pump} = 258$ nm at selected fluorescence wavelengths. Open symbols: Experimental data points. Solid lines: Fitted curves. The insets show the rise of the fluorescence at $\lambda_{fl} = 510$ and 500 nm, respectively, at the two pump wavelengths measured with respect to fluorescein 27 and rhodamine 6G.

emission wavelengths with $\lambda_{pump} = 258$ nm in Figure 3b. To our surprise, the respective curves at comparable fluorescence wavelengths are remarkably similar. No significant dependences of the exponential decay times on λ_{pump} were observable within the experimental uncertainties, when the respective data curves were individually fitted aside from some changes of the relative fractional amplitudes. Moreover, the insets in Figure 3a and b show the respective rise curves of the emissions of DMAde in the red compared to fluorescein 27 and rhodamine 6G as standards. As can be seen, although the data at $\lambda_{pump} = 294$ nm are somewhat noisy, the red-shifted fluorescence of DMAde appears promptly after the pump pulse without noticeable time lag within the experimental resolution at both excitation wavelengths, that is, even after excitation close to the electronic origin.

With these premises, all fluorescence decay curves of DMAde in water were subjected to a joint global fit as described in the Experimental Section to determine the values of the set of time constants describing the observed dynamics. The results are compiled in Table 1. All fluorescence decay profiles over the range of $350 \leq \lambda_{fl} \leq 510$ nm could be fitted with three exponentials with the time constants

$$\tau_2 = 0.52 \pm 0.03 \text{ ps}$$
$$\tau_4 = 3.0 \pm 0.2 \text{ ps}$$
$$\tau_5 = 62.0 \pm 1.0 \text{ ps}$$

independent of λ_{pump} within the 2σ error limits. A major additional process was monitored in the very blue fluorescence decay profiles measured with $\lambda_{pump} = 258$ nm. Here, we found an ultrafast process taking place at $\lambda_{fl} = 300$ and 310 nm on a time scale of

$$\tau_1 < 0.1 \text{ ps}$$

faster than our experimental time resolution[56] but slowed down to

$$\tau_1 = 0.22 \pm 0.03 \text{ ps}$$

at $\lambda_{fl} = 320$ nm. Furthermore, the best fit required a slightly shorter time constant of

$$\tau_3 = 1.5 \pm 0.1 \text{ ps}$$

instead of $\tau_4 = 3.0 \pm 0.2$ ps. The 1.5 ps value was also encountered in the traces at $\lambda_{fl} = 550$ and 650 nm, where it will be referred to below as τ_3' when required.

3.2.2. DMAde in Dioxane. The temporal fluorescence profiles of DMAde in dioxane were studied following excitation at $\lambda_{pump} = 258$, 285, and 294 nm. The measured decay curves for $\lambda_{pump} = 258$ nm at 13 fluorescence wavelengths in the range of $290 \leq \lambda_{fl} \leq 540$ nm are displayed in Figure 4a up to $\Delta t = 10$ ps and in Figure 4b up to $\Delta t = 750$ ps. The differences between the time profiles at UV wavelengths compared to those in the visible spectrum are even more striking than those in water before. At $\lambda_{fl} < 370$ nm, the mean fluorescence lifetime is on the order of $\langle\tau\rangle \approx 1$ ps or below, whereas the decay times at visible wavelengths extend to $\tau > 1$ ns.

Five fluorescence wavelengths between $350 \leq \lambda_{fl} \leq 510$ nm were probed using $\lambda_{pump} = 285$ and 294 nm. A comparison of the time profiles with $\lambda_{pump} = 258$ and 294 nm is given in Figure 5. As it turned out, all decay curves at corresponding emission wavelengths resembled each other.

The applied global fit procedure revealed dynamic processes occurring on five distinctive time scales. In particular, apart from an ultrafast process with a decay time of

$$\tau_1 = 0.27 \pm 0.02 \text{ ps}$$

detected only at the shortest fluorescence wavelength ($\lambda_{fl} = 290$ nm) with $\lambda_{pump} = 258$ nm, all profiles could be described with time constants ($\pm 2\sigma$ standard deviations) of

$$\tau_2 = 0.63 \pm 0.04 \text{ ps}$$
$$\tau_3 = 1.5 \pm 0.1 \text{ ps}$$
$$\tau_4 = 10.9 \pm 1.0 \text{ ps}$$
$$\tau_5 = 1400 \pm 38 \text{ ps}$$

irrespective of the value of λ_{pump}. The fit results are compiled in Table 2.

3.3. Fractional Spectral Amplitudes. The fractional spectral amplitudes determined by the fits encode information on the

TABLE 1: Experimental Fluorescence Decay Times and Relative Amplitudes of DMAde in Water Obtained from a Global Fit (2σ standard deviation with respect to the last digits in parentheses)

λ_{pump} (nm)	λ_{fl} (nm)	τ_1 (ps)	a_1	τ_2 (ps)	a_2	τ_3 (ps)	a_3	τ_4 (ps)	a_4	τ_5 (ps)	a_5
258	300	<0.1	0.98(4)			1.5(1)	0.02(1)				
	310	<0.1	0.97(4)			1.5(1)	0.03(1)				
	320	0.22(3)	0.83(6)			1.5(1)	0.17(3)			62(1)	<0.01
	350			0.52(3)	0.81(3)			3.0(2)	0.18(2)	62(1)	0.01(1)
	420			0.52(3)	0.57(2)			3.0(2)	0.42(2)	62(1)	0.01(1)
	450			0.52(3)	0.36(4)			3.0(2)	0.59(3)	62(1)	0.05(1)
	500			0.52(3)	0.37(4)			3.0(2)	0.49(2)	62(1)	0.14(1)
	550					1.5(1)	0.50(2)			62(1)	0.50(1)
	600					1.5(1)	0.25(1)			62(1)	0.75(1)
	650									62(1)	1.00(1)
294	350			0.52(3)	0.87(4)			3.0(2)	0.12(2)	62(1)	0.01(1)
	369			0.52(3)	0.70(4)			3.0(2)	0.29(3)	62(1)	0.01(1)
	410			0.52(3)	0.55(5)			3.0(2)	0.45(3)	62(1)	0.01(1)
	433			0.52(3)	0.33(5)			3.0(2)	0.65(3)	62(1)	0.01(1)
	446			0.52(3)	0.37(5)			3.0(2)	0.61(3)	62(1)	0.02(1)
	510			0.52(3)	0.23(5)			3.0(2)	0.53(3)	62(1)	0.23(1)

character and sequence of the states that are reached in the ensuing electronic relaxation. In an ideal case, each decay component would reflect a distinctive state, although such a simple picture is blurred by strong couplings. Nevertheless, the spectral amplitudes provide valuable hints toward meaningful assignments.

3.3.1. DMAde in Water. The fractional spectral amplitudes of the decay components of DMAde in water excited at $\lambda_{pump} = 258$ nm are plotted versus the fluorescence wavelength in Figure 6. Starting in the UV, an ultrafast initial switch from $\tau_1 \leq 0.22$ ps to $\tau_2 = 0.52$ ps is evident between $\lambda_{fl} = 300$ and 350 nm. Subsequently, a switch occurs from τ_2 as the main decay component in the range of $350 \leq \lambda_{fl} \leq 500$ nm (peak at $\lambda_{fl} = 360$ nm) to $\tau_4 = 3.0$ ps, which extends over the range of $350 \leq \lambda_{fl} \leq 500$ nm (peak at $\lambda_{fl} = 450$ nm), or from τ_2 to $\tau_3' = 1.5$ ps (up to $\lambda_{fl} \leq 600$ nm) and eventually to $\tau_5 = 62$ ps, which dominates the fluorescence decay profiles at the most red-shifted wavelengths. The decay times τ_3,$\tau_3' = 1.5$ ps and $\tau_4 = 3$ ps are too close to each other to be clearly separated. However, as will be argued in the Discussion, τ_1 may be attributed to the motion of the excited wavepacket away from the Franck−Condon region in the optically bright $\pi\pi^*(L_a)$ state, τ_2 to the direct deactivation of the $\pi\pi^*(L_a)$ state, τ_3/τ_4 to the $\pi\pi^*(L_b)$ state, and τ_5 to the CT state.

The respective spectral amplitudes encountered with $\lambda_{pump} = 294$ nm are less complete because only six fluorescence wavelengths were measured at that pump wavelength, but they show a quite similar trend (see Table 1). Only the very fast first component (τ_1) is missing when the molecules are excited just barely to their electronic origin.

3.3.2. DMAde in Dioxane. The fractional spectral amplitudes for DMAde in dioxane following $\lambda_{pump} = 258$ nm are given in Figure 7. As can be seen, the decays are initially dominated by $\tau_2 = 0.63$ ps at the shorter λ_{fl} ($300 \leq \lambda_{fl} \leq 350$ nm), but $\tau_3 = 1.51$ ps becomes the main time constant in the range of $365 \leq \lambda_{fl} \leq 490$ nm. The latter component has significant amplitude in the entire range of the fluorescence spectrum. Furthermore, while $\tau_4 = 10.9$ ps remains a minor component and is detectable only in the range of $400 \leq \lambda_{fl} \leq 500$ nm, significant contributions from $\tau_5 = 1400$ ps first arise at $\lambda_{fl} \approx 410$ nm, grow in with increasing λ_{fl}, and eventually dominate at $\lambda_{fl} \gtrsim 500$ nm. After $\lambda_{pump} = 294$ nm, on the other hand, the fastest

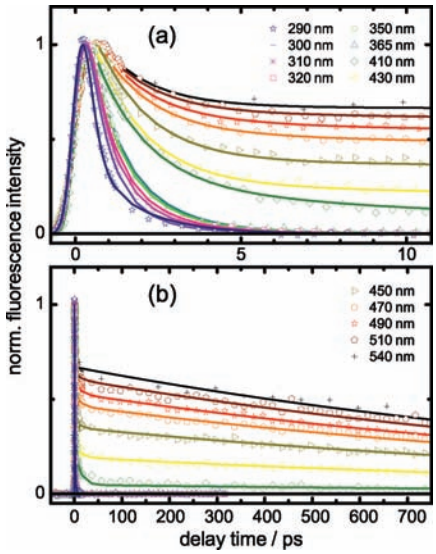

Figure 4. Normalized fluorescence decay profiles of DMAde in dioxane excited at $\lambda_{pump} = 258$ nm at different fluorescence wavelengths in the range of $290 \leq \lambda_{fl} \leq 540$ nm. Open symbols: Experimental data points. Solid lines: Fitted curves from global data analysis.

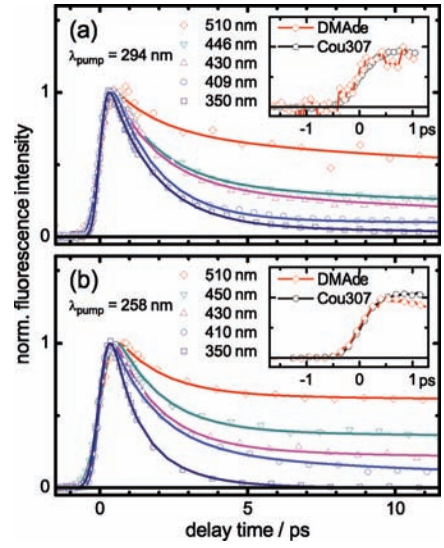

Figure 5. Comparison of the fluorescence time profiles of DMAde in dioxane excited at λ_{pump} = (a) 294 and (b) 258 nm at selected fluorescence wavelengths. Open symbols: Experimental data points. Solid lines: Fitted curves. The insets show the rise of the fluorescence at $\lambda_{fl} = 510$ nm at the two pump wavelengths measured with respect to coumarin 307.

TABLE 2: Experimental Fluorescence Decay Times and Relative Amplitudes of DMAde in Dioxane Obtained from a Global Fit (2σ standard deviation with respect to the last digits in parentheses)

λ_{pump} (nm)	λ_{fl} (nm)	τ_1 (ps)	a_1	τ_2 (ps)	a_2	τ_3 (ps)	a_3	τ_4 (ps)	a_4	τ_5 (ps)	a_5
258	290	0.27(2)	0.82(3)			1.51(3)	0.18(2)				
	300			0.63(4)	0.86(5)	1.51(3)	0.17(3)				
	310			0.63(4)	0.75(5)	1.51(3)	0.26(5)				
	320			0.63(4)	0.66(5)	1.51(3)	0.35(5)				
	350			0.63(4)	0.52(5)	1.51(3)	0.48(4)			1400(38)	<0.01
	365			0.63(4)	0.45(5)	1.51(3)	0.55(4)			1400(38)	<0.01
	409					1.51(3)	0.91(2)	10.9(1)	0.02(2)	1400(38)	0.07(1)
	430					1.51(3)	0.79(2)	10.9(1)	0.07(2)	1400(38)	0.15(1)
	450					1.51(3)	0.70(2)	10.9(1)	0.04(2)	1400(38)	0.26(1)
	470					1.51(3)	0.57(2)	10.9(1)	0.06(2)	1400(38)	0.37(1)
	490					1.51(3)	0.51(2)	10.9(1)	0.07(2)	1400(38)	0.43(1)
	510					1.51(3)	0.47(2)	10.9(1)	0.03(2)	1400(38)	0.50(1)
	540					1.51(3)	0.45(2)			1400(38)	0.56(1)
285	350			0.63(4)	0.15(5)	1.51(3)	0.85(4)			1400(38)	0.01(1)
	369			0.63(4)	0.32(5)	1.51(3)	0.68(4)			1400(38)	0.01(1)
	405					1.51(3)	0.91(2)	10.9(1)	0.06(2)	1400(38)	0.04(1)
	490					1.51(3)	0.47(2)	10.9(1)	0.15(2)	1400(38)	0.38(1)
	510					1.51(3)	0.40(2)	10.9(1)	0.11(2)	1400(38)	0.49(1)
294	350					1.51(3)	0.93(2)	10.9(1)	0.06(2)	1400(38)	0.01(1)
	410					1.51(3)	0.78(2)	10.9(1)	0.18(2)	1400(38)	0.04(1)
	430					1.51(3)	0.69(2)	10.9(1)	0.22(2)	1400(38)	0.10(1)
	446					1.51(3)	0.68(2)	10.9(1)	0.17(2)	1400(38)	0.15(1)
	510					1.51(3)	0.35(3)	10.9(1)	0.26(2)	1400(38)	0.39(1)

processes (τ_1 and τ_2) are missing, and the time profiles are characterized by τ_3, τ_4, and τ_5 only (see Table 2). The component τ_3 governs at $\lambda_{fl} < 450$ nm, and τ_5 predominates at the most red-shifted λ_{fl}.

3.4. Reconstructed Transient Fluorescence Spectra. The transient emission spectra which we can reconstruct[48,52−54] from the measured fluorescence decay profiles reflect the ensuing molecular relaxation dynamics initiated by the pump pulse via possible intermediates to the ground state by time-dependent spectral evolutions.

3.4.1. DMAde in Water. The reconstructed transient fluorescence spectra of DMAde in water at selected time slices are given in Figure 8a. As can be seen, the emission in the first few picoseconds shows an intense peak in the UV, but even at the shortest times, the spectra have a long tail extending over the entire wavelength range into the red and appearing without detectable time delay, as was already demonstrated by the rise curves in Figure 5.

In order to highlight the ensuing spectral evolutions, we normalized the traces with respect to their maxima as shown in Figure 8b and c. Considerable changes are revealed on different time scales. (i) At the shortest times ($\Delta t \leq 0.15$ ps, Figure 8b), there is a clear spectral shift from $\lambda_{fl} = 310$ to 320 nm already

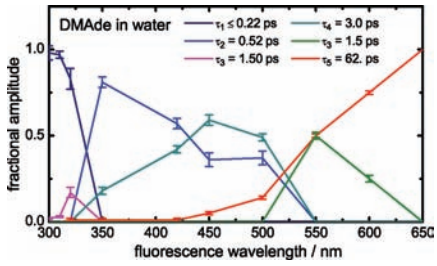

Figure 6. Plot of the fractional spectral amplitudes from the global fit to the measured fluorescence decay profiles of DMAde in water at $\lambda_{pump} = 258$ nm versus the fluorescence wavelength.

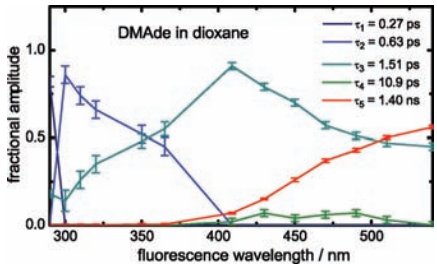

Figure 7. Plot of the fractional spectral amplitudes from the global fit to the measured fluorescence decay profiles of DMAde in dioxane at $\lambda_{pump} = 258$ nm versus the fluorescence wavelength.

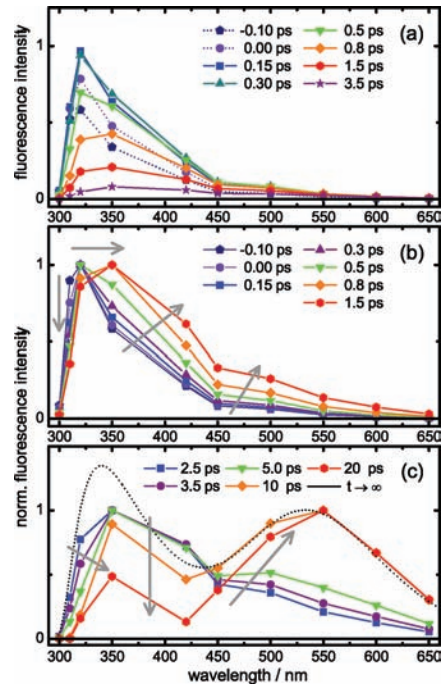

Figure 8. Reconstructed transient emission spectra of DMAde in water. (a) Spectral intensities at a number of different time slices. (b, c) Normalized transient spectra at early ($\Delta t \leq 1.5$ ps, b) and longer times (up to $\Delta t = 20$ ps, c). Arrows indicate the temporal spectral changes. The scaled static fluorescence spectrum is included in the lower panel for comparison.

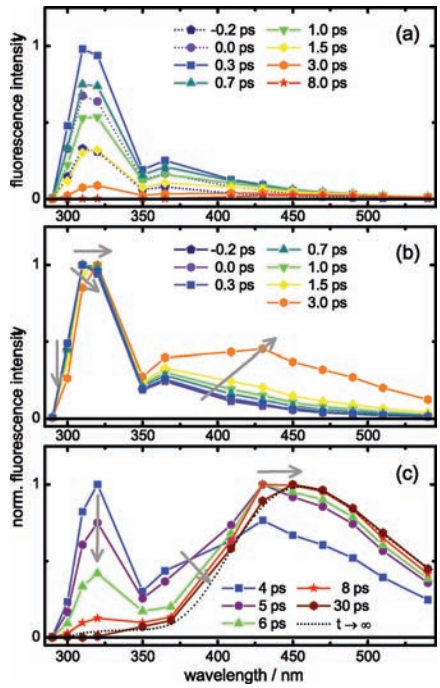

Figure 9. Reconstructed transient emission spectra of DMAde in dioxane. (a) Spectral intensities at a number of different time slices. (b, c) Normalized transient spectra at early ($\Delta t \leq 3$ ps, a) and at longer times ($\Delta t \leq 30$ ps, b). Arrows indicate the temporal spectral changes. The scaled static fluorescence spectrum is included in the lower panel for comparison.

within the duration of the pump pulse; (ii) immediately thereafter, in a time up to $\Delta t \approx 0.8$ ps, the maximum of the UV band shifts further to $\lambda_{fl} \approx 350$ nm, about the peak wavelength of the UV band in the static fluorescence spectrum. (iii) The intensity at these early times extends from the UV into the visible without a distinctive spectral signature in the red. (iv) After $\Delta t \approx 5-10$ ps (Figure 8c), the UV and visible emission bands appear roughly equally balanced, and the maximum of the emission band in the visible finally settles at $\lambda_{fl} = 550$ nm. (v) For $\Delta t \geq 10$ ps, the transient emission spectrum matches the static fluorescence spectrum for the A band (dotted line), and no further spectral evolution occurs.

3.4.2. DMAde in Dioxane. The reconstructed transient emission spectra of DMAde in dioxane at selected time slices are given in Figure 9a. As before, the emission at the shortest times peaks in the UV, but the spectrum has a long tail reaching into the visible. The normalized transient spectra in Figure 9b and c highlight the ensuing spectral shifts. (i) At the earliest time, the intensity maximum is at $\lambda_{fl} = 310$ nm, but the 310 nm signal decays rapidly, and the maximum shifts to $\lambda_{fl} = 320$ nm within $\Delta t < 3.0$ ps. (ii) The drop in the UV is accompanied by a gain of red-shifted emission, which outruns the UV band after $\Delta t \approx 5$ ps. (iii) In the next ~10 ps, the maximum shifts to $\lambda_{fl} = 450$ nm. (iv) At $\Delta t \geq 30$ ps, the emission at $\lambda_{fl} \leq 325$ nm has disappeared, and the emission in the visible region finally matches the static fluorescence spectrum shown in Figure 9c by the dotted line.

4. Discussion

In the preceding section, we established a firm experimental basis regarding the fluorescence lifetimes of the dual fluorescence molecule DMAde at many different emission wavelengths covering the entire spectrum from the UV to the red after femtosecond excitation close to the electronic origin and to vibronic energies well beyond. The ultrafast radiationless electronic relaxation dynamics of the molecules were studied in two prototypical solvents, the polar protic water and the nonpolar aprotic dioxane. In this section, we attempt to develop a consistent model to rationalize the observed dynamics, building on the available body of experimental[2−9] and theoretical[28−38] information on the parent molecule Ade.

4.1. Measured Fluorescence Decay Time Constants. The main findings to this point can be summarized as follows.

(i) All satisfactory fits to the observed fluorescence−time profiles of DMAde in water and in dioxane require several exponentials. The contributions of the distinctive decay components depend on the fluorescence wavelength. Furthermore, the values of the time constants depend on the solvent.

(ii) A striking feature with both solvents is that the time constants describing the electronic deactivation are identical within our experimental errors, irrespective of whether the molecules were measured high above ($\lambda_{pump} = 258$ nm) or close to their electronic origin ($\lambda_{pump} = 294$ nm). The only noteworthy difference is the absence of the fastest events in the molecules near the origin; those processes are encountered only after excitation to higher vibronic energies and then only at the shortened fluorescence wavelengths in the UV. Otherwise, similar relaxation pathways appear to be available to the molecules with little or with high initial excess excitation energies.

(iii) Specific dynamic processes were identified on five well-defined times scales. The time constants $\tau_1-\tau_5$ each predominate in different spectral regions. Together with the observed large Stokes shifts up to $\Delta\nu \approx 15000$ cm^{-1} in the static (Figure 1) and the transient fluorescence spectra (Figures 8 and 9), we conclude that more than one intermediate excited state is involved in the deactivations.

(iv) The initial electronic relaxation processes in the DMAde molecules take place generally somewhat more slowly in the nonpolar aprotic solvent dioxane than in the polar protic water. A huge difference is encountered, however, for the most red-shifted fluorescence, where the lifetime increases from $\tau_5 = 62$ ps in water to 1400 ps in dioxane. That effect explains the strong prominence of the visible over the UV emission band in the static fluorescence spectrum of DMAde in dioxane (compare Figure 1c). The eventual deactivation of the red state back to the ground state must depend strongly on the environment of the DMAde molecules.

(v) The measurements of the rise times of the red-shifted fluorescence from DMAde relative to selected laser dyes as reference clocks demonstrate the absence of any noticeable time delay of the emission in the red with respect to the pump pulse within the experimental time resolution in both solvents. The "red state" seems to be virtually promptly populated. The reconstructed transient fluorescence spectra illustrate, in some detail, how the emissions in the UV and the visible arise. It has to be taken into account, however, that the large width of the intense UV emission band at short times, when it extends to long wavelengths well into the visible spectrum (see Figures 8 and 9), may obscure some delayed weaker emissions from sequential transitions between the involved excited states. The characteristic spectral band structure of the red state is developed only after a few picoseconds.

(vi) In both solvents, already the fluorescence−time profiles in the UV exhibit some small but non-negligible contributions from the long-lived ($\tau_5 = 62$ ps respectively 1400 ps) red state. In particular, discernible spectral amplitudes from τ_5 were first noted in the time profiles at $\lambda_{fl} \approx 350$ nm and became clearly

obvious at $\lambda_{fl} > 450$ nm in water and >405 nm in dioxane (see Tables 1 and 2).

4.2. Electronic Deactivation Pathways in the Parent Molecule Ade. As a starting point for a suitable model for the electronic dynamics in DMAde, we turn to the parent molecule Ade, which constitutes the chromophore. The ground-state π electron configurations of both molecules are the same, and apart from a small shift to lower energies due to the two methyls at the exocyclic amino N atom, the initial excited states of Ade and DMAde that are reached by the femtosecond UV pump pulses should be very similar as well. For the case of Ade, it is well-known that we have to consider at least three low-lying, nearly isoenergetic singlet excited states, namely, the optically accessible $\pi\pi^*(L_b)$ and $\pi\pi^*(L_a)$ states and the optically forbidden $n\pi^*$ state.

4.2.1. 9H-Ade. The $\pi\pi^*(L_a)$ state is the third excited state of 9H-Ade in vacuo, but it is stabilized in the dielectric environment of the solvent relative to the $\pi\pi^*(L_b)$ and $n\pi^*$ states by its higher dipole moment. In water, it is therefore almost isoenergetic with the $\pi\pi^*(L_b)$ state. Since it carries the bulk of the oscillator strength, it is the initially excited state at all pump wavelengths except right at the origin of the strong first UV absorption band of 9H-Ade, where the $\pi\pi^*(L_b)$ state contributes.

Available high-level ab initio calculations agree[29−31,34−36,38] that the $\pi\pi^*(L_a)$ PEHS has a repulsive character with a steep potential energy gradient in the Franck−Condon (FC) region and that the subpicosecond deactivation ($\tau \approx 0.3$ ps in water[8] and ∼0.38 ps in dioxane[57]) is determined by an ultrafast barrierless pathway through a direct CI with the S_0 state involving a large-amplitude puckering motion of the C^2H group of the purine ring. Relaxation through $\pi\sigma^*$ excited states involving the N^9H or NH_2 groups or ring-opening reactions[28−30] appear to come into play only at shorter excitation wavelengths than those of interest here. Along the minimum-energy pathway (MEP) to the C^2H puckering CI with the S_0 state, the $\pi\pi^*(L_a)$ state crosses the $\pi\pi^*(L_b)$ and $n\pi^*$ states. In this region, where the three excited states are strongly mixed and their characters are therefore not easily distinguishable, the ab initio calculations vary in detail but not in their essential conclusions. Serrano-Andrés et al.[36,43] argue that the $\pi\pi^*(L_a)$ state leads directly to the C^2H puckering CI with S_0, while Marian,[31] Blancafort,[35] and Barbatti and Lischka[38] suggest relaxation via a sequence of ultrafast transformations from $\pi\pi^*(L_a)$ to $\pi\pi^*(L_b)$ and $n\pi^*$ to the C^2H puckering CI. Pointing at the distinctive, partially localized characters of the two singly occupied molecular orbitals at the CI, Zgierski et al.[58] refer to this pathway as the biradical channel. In vacuo, part of the excited wavepacket in Ade en route to the S_0 state can be trapped in the shallow $n\pi^*$ potential energy well, explaining the observed longer ($\tau \approx 1$ ps) lifetime component.[23,59] In solution, however, where the $\pi\pi^*(L_a)$ state is lowered and the $n\pi^*$ state is raised, as is relevant for us here, the wavepacket returns essentially directly to the S_0 state, regardless of whether the initial excitation was to the $\pi\pi^*(L_a)$ or $\pi\pi^*(L_b)$ state and without being caught for more than 100−300 fs in some excited state potential minimum.

4.2.2. 7H-Ade. In addition to 9H-Ade, it is instructive to look at the 7H-Ade tautomer because it showcases an astonishing diversity in the excited-state deactivation. With $\tau \approx 8$ ps in aqueous solution,[8] or ∼15 ps in dioxane,[57] its electronic lifetime is considerably longer than that of the canonical 9H form. Indeed, the available ab initio calculations[36,37] propose that the optically excited wavepacket on the $\pi\pi^*(L_a)$ PEHS follows its MEP only to a local minimum, where the $\pi\pi^*(L_a)$ state is almost isoenergetic with the $\pi\pi^*(L_b)$ and $n\pi^*$ states, and a fast switching to those states takes place. Direct deactivation to S_0 through the C^2H puckering biradical CI is therefore disfavored. Instead, the wavepacket is trapped in the $\pi\pi^*(L_b)$ and/or $n\pi^*$ wells, giving rise to the observed longer lifetimes. The biradical CI that determines the fate of the excited state in the 9H case cannot be reached from those minima without a significant activation energy. The same is true for an $n\pi^*/S_0$ CI involving bending of the amino group, which has been proposed to be responsible for the eventual deactivation of the 7H-Ade.[36]

Interestingly, the structure of 7H-Ade in the global $S_1(n\pi^*)$ minimum differs from that of 9H-Ade in that the amino group is twisted by 90° with respect to the purine plane.[36,37] Furthermore, when the molecule becomes nonplanar in some calculated local minima on the excited PEHS, the nominally forbidden $n\pi^*-S_0$ transition can gain some oscillator strength.[37]

4.3. Electronic Deactivation of DMAde. Turning to DMAde, we have to consider the same three excited states as in Ade, that is, $\pi\pi^*(L_a)$, $\pi\pi^*(L_b)$, and $n\pi^*$. In addition, the experimental results point at the existence of a fourth state that is responsible for the long-lived long-wavelength fluorescence far into in the visible spectrum (coined above as the red state for simplicity). The strong bathochromic shift[44,45] of the peak emission wavelength upon going from nonpolar to polar solvents (see Figure 1, for example) suggests that the state of interest possesses a large dipole moment, as would be expected to arise from an intramolecular charge transfer (ICT). In line with the literature on DMAde, we shall therefore refer to the red-emitted state in the following as the ICT state. Even though its electronic structure and geometry have not been as well characterized when compared to the large body of calculations on Ade, the ICT picture is supported by semiempirical INDO/S[45] and CISD ab initio calculations.[46] We note, nevertheless, that we cannot a priori rule out a possible implication of some other long-lived excited state than an ICT species carrying a small but non-negligible oscillator strength and having a structure differing from that of the ground state (e.g., some $n\pi^*$ configuration) in a way that its fluorescence falls into the visible range of the spectrum with the observed large Stokes shift. With these premises, we propose a four-state model for the dynamics of DMAde, as depicted in Figure 10.

4.3.1. Ultrafast Relaxation of the Franck−Condon State. From Ade, we can safely conclude that vertical excitation of DMAde with a short-wavelength UV pump pulse (e.g., $\lambda_{pump} = 258$ nm) should prepare the molecules in the optically bright $\pi\pi^*(L_a)$ state, which carries most of the oscillator strength. At the short pump wavelengths, the molecules receive a sizable excess energy above the $\pi\pi^*$ origin. Under those conditions, the fastest dynamic processes were detected at the shortest fluorescence wavelengths, $\lambda_{fl} = 300$ and 310 nm in water (w). The observed decay on the time scale of $\tau_{1,w} < 0.1$ ps at those wavelengths is therefore assigned to the immediate departure of the excited wavepacket from the FC region. Indeed, the amplitude at $\lambda_{fl} \leq 310$ nm in the transient fluorescence spectra decays within the duration of the pump pulse. The experimental observations are in full agreement with a steep gradient and repulsive character of the excited PEHS in the FC region. With longer pump wavelengths, we can no longer reach that steep part of the PEHS.

The initial departure from the FC region faster than our experimental time resolution seems to be essentially over after ∼0.2−0.3 ps. At $\lambda_{fl} = 320$ nm, we already measured a fluorescence lifetime of $\tau_{1,w} \approx 0.22$ ps in water. Likewise, the fastest processes in dioxane (d), where the $\pi\pi^*(L_a)$ state is higher in energy than that in water, were observed to take a

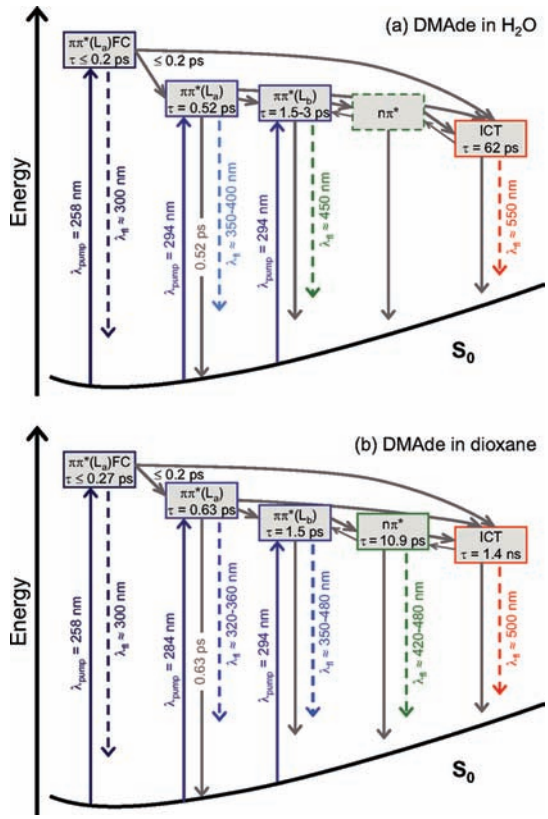

Figure 10. Simplified four-state model for the electronic dynamics of DMAde in water (a) and dioxane (b). The different energies of the involved states due to the ensuing solvent shifts are indicated by their relative positions. The employed pump transitions to the two $\pi\pi^*$ states and the respective relaxation pathways of the excited states are indicated by solid lines, and the fluorescence from the states with their approximate peak wavelengths are indicated by dashed lines.

time of $\tau_{1,d} \approx 0.27$ ps, observed at $\lambda_{fl} = 290$ nm. Parallel with τ_1, we observe the onset of decay components with $\tau_3 \approx 1.5$ ps in both solvents, indicating that a region on the $\pi\pi^*(L_a)$ PEHS is reached by the wavepacket, where part of it is trapped for a short time.

4.3.2. Radiationless Deactivation of the $\pi\pi^*(L_a)$ State. Considering the DMAde fluorescence at wavelengths over the range of $320 \leq \lambda_{fl} \leq 510$ nm, we have to account for contributions from two decay constants. Their values in water are $\tau_{2,w} = 0.52$ ps and $\tau_{4,w} = 3.0$ ps. Both processes were observed with $\lambda_{pump} = 258$ nm as well as with $\lambda_{pump} = 294$ nm. At somewhat shorter or longer fluorescence wavelengths, for $\lambda_{pump} = 258$ nm, we obtained $\tau_{3,w} = 1.5$ ps (respectively, $\tau'_{3,w} = 1.5$ ps) instead of $\tau_{4,w}$. DMAde in dioxane has almost identical time constants ($\tau_{2,d} = 0.63$ ps and $\tau_{3,d} = 1.51$ ps) in the fluorescence wavelength range of $300 \leq \lambda_{fl} \leq 370$ nm, but the shorter $\tau_{2,d}$ is encountered only with short pump wavelengths ($\lambda_{pump} = 258$ and 285 nm), not after excitation at $\lambda_{pump} = 294$ nm close to the $\pi\pi^*$ origin. In view of the similar magnitudes of those τ_2 values with the 0.3 and 0.38 ps fluorescence lifetimes of the parent molecule Ade in water and dioxane, respectively, $\tau_{2,w}$ and $\tau_{2,d}$ are attributed to the direct deactivation of the wavepacket from the $\pi\pi^*(L_a)$ state to S_0 through the C^2H puckering biradical CI. The absence of the 0.58 ps component for DMAde in dioxane excited at $\lambda_{pump} = 294$ nm (and its small spectral amplitude at $\lambda_{pump} = 284$ nm) is a consequence of the fact that the pump pulses at those wavelengths reach merely the $\pi\pi^*(L_b)$ rather than the slightly higher $\pi\pi^*(L_a)$ state.

Taking the radiative lifetime of $\tau_r \approx 2$ ns for the LE state determined at 80 K[44] and combining it with our measured τ_2 values, we estimate UV fluorescence quantum yields of DMAde in the B bands of $\Phi_{fl,B} = 2.6 \times 10^{-4}$ in water and 3.2×10^{-4} in dioxane, in surprisingly excellent agreement with the reported experimental values.[44,45] Hence, the UV fluorescence seems to be limited by the ultrafast direct radiationless electronic deactivation rate of the optically bright $\pi\pi^*(L_a)$ state to S_0 through the biradical CI. The probable shallow local potential energy minimum of the $\pi\pi^*(L_a)$ state along the MEP to that CI does not seem to capture and hold (see below) more than a small part of the wavepacket.

4.3.3. Lifetime of the $\pi\pi^*(L_b)$ State. The decay constants $\tau_{2,w} = 0.52$ ps and $\tau_{4,w} = 3$ ps in the spectral region of $320 \leq \lambda_{fl} \leq 550$ nm (or $\tau_{3,w}, \tau'_{3,w} = 1.5$ ps just outside of this region) for DMAde in water seem to be linked to each other because they do not only share the same spectral region, but it is also the case that $\tau_{2,w}$ has its maximal amplitude where $\tau_{4,w}$ has its minimal amplitude and vice versa. The importance of $\tau_{4,w}$ grows with longer λ_{fl}. The same is true for $\tau_{2,d} = 0.63$ ps and $\tau_{3,d} = 1.5$ ps over the range of $300 \leq \lambda_{fl} \leq 370$ nm for DMAde in dioxane. The anticorrelation of the respective spectral amplitudes suggests some precursor−product relationship. As a plausible explanation, we assume that a small part of the excited wavepacket initially en route to the biradical CI is first caught in the region of the $\pi\pi^*(L_a)$ minimum and then trapped in the $\pi\pi^*(L_b)$ well. The deactivation from this local minimum thereafter can proceed only across a shallow potential energy barrier, which needs to be overcome and therefore slows the dynamics. This part of the proposed picture for DMAde is very similar to that described for the case of 7H-Ade.[36,37]

Indeed, Zgierski et al.[58] point out a destabilization in DMAde compared to Ade of the biradical state that is responsible for the direct deactivation of the $\pi\pi^*$ to the S_0 state through the C^2H puckering CI and the development of a potential energy barrier along the MEP. The barrier seems to be sufficiently high to support a number of bound vibrational states in the well. This important difference to Ade fully explains the long fluorescence lifetime (~2 ns) of DMAde observed at 80 K.[44] Furthermore, in the case of DMAde in dioxane excited at $\lambda_{pump} = 294$ nm, the pump pulses seem to project a wavepacket from S_0 essentially directly into this $\pi\pi^*(L_b)$ minimum.

The difference between the time constants $\tau_{3,w} \approx 1.5$ ps and $\tau_{4,w} = 3$ ps observed in water is small, and it is not certain that these values are really physically distinct. Interestingly, $\tau_{4,w}$ appears when $\tau_{3,w}$ vanishes, and $\tau'_{3,w}$ appears when $\tau_{4,w}$ disappears. We can only note that tentative fits, in which we attempted to combine both lifetimes in a single decay component, did not satisfactorily represent the experimental data. We tend to ascribe this phenomenon to coinciding parallel or sequential relaxation processes involving different local minima on the global PEHS. As already mentioned, the $\pi\pi^*(L_a)$, $\pi\pi^*(L_b)$, and $n\pi^*$ states in the region of the local $\pi\pi^*(L_a)$ minimum likely are strongly mixed. However, different vibrational or vibronic excess energies may play a role as well. We cannot say whether the wavepacket trapped in the $\pi\pi^*(L_b)$ well eventually deactivates to S_0 or whether it transforms to the ICT state, although the latter case appears likely.

4.3.4. The $n\pi^*$ State. The $n\pi^*$ state should normally be optically dark and therefore forbidden in the fluorescence spectrum, but it can pick up some oscillator strength in nonplanar configurations.[31,37] Although conclusions on the $n\pi^*$ state have to be handled with great caution, it is possible that the presence of strong couplings between the $n\pi^*$ and $\pi\pi^*(L_b)$ states and the existence of several local excited-state minima may lead to weak, red-shifted fluorescence from regions of the PEHS of

mixed electronic character. It is striking that the spectral amplitude over the range of $400 \leq \lambda_{fl} \leq 500$ nm associated with the time constant $\tau_{4,d} = 10.9$ ps for DMAde in dioxane (Figure 7) begins to rise just at the maximum of $\tau_{3,d}$. Hence, $\tau_{4,d}$ might tentatively be attributed to such a mixed $n\pi^*/\pi\pi^*(L_b)$ case. A direct counterpart for $\tau_{4,d}$ in water appears to be hidden. However, we notice that the excited-state lifetime of $\tau \approx 15$ ps for 7H-Ade in dioxane[57] is of the same magnitude.

4.3.5. Long-Wavelength Fluorescence from the ICT State. Following the literature,[44−46] on the basis of the experimental evidence, the distinctive long-wavelength A band in the fluorescence spectrum of DMAde is assigned to the formation of an ICT state. That state has no counterpart in Ade. As mentioned, the ICT character is deduced from the pronounced bathochromic shift from the nonpolar solvent dioxane to the polar water. The rise time measurements and the transient fluorescence spectra show that long-wavelength emission can be observed immediately after the pump pulse; it is present already at the earliest relaxation times. This seems to be the case even after excitation at $\lambda_{pump} = 294$ nm close to the $\pi\pi^*$ origin. Our time-resolved measurements thus appear to suggest a superfast, direct population from the optically bright state within $\lesssim$100 fs. We nevertheless hesitate to draw this as a definite conclusion from our data. The main reason is that the intense long-wavelength tail of the strong emission from the FC, the $\pi\pi^*(L_a)$, and (weaker) from the $\pi\pi^*(L_b)$ states, which is clearly visible in our time-resolved emission spectra in Figures 8 and 9 within the first ∼2−3 ps after the pump pulse, may obscure a slower, sequential population of the ICT state. Thus, a transition to the ICT state on the few picosecond time scale by sequential relaxation from the FC via the $\pi\pi^*(L_a)$ and/or $\pi\pi^*(L_b)$ states is a possibility that cannot be ruled out from our data. Second, a direct $\pi\pi^*(FC) \rightarrow$ ICT transformation and a sequential mechanism may as well run parallel. In that case, where the FC-excited wavepacket would decay mostly to the local $\pi\pi^*(L_a)$ minimum and then on to S_0 and only a small part would branch to the ICT state, the ultrafast rise of the red emission would just reflect the ultrafast decay of the FC state. Obviously, however, the distinctive fluorescence band of the ICT state is well developed after no less than $\Delta t \approx 4-5$ ps and dominates the emission spectrum thereafter.

The lifetimes of the ICT states are far longer than those of the two $\pi\pi^*$ states. For DMAde in water, we found a value of $\tau_{5,w} = 62$ ps, which still indicates the existence of a fast and efficient radiationless deactivation mechanism. In dioxane, however, the ICT state was found to have a lifetime of $\tau_{5,d} = 1400$ ps. Several points come to mind. (i) It is likely that the energy of the ICT state at a CI linking it with S_0 is lowered in the polar solvent water such that the deactivation is accelerated to the observed rate. (ii) The early spectral onset of the long (τ_5) decay component attributed to the ICT state already below $\lambda_{fl} \approx 450$ nm in water and below 405 nm in dioxane either shows that the ICT state must have an unusually broad FC emission range or it hints at a reversible ICT transformation (depending on the solvent). A slow (thermal) reversibility of a $\pi\pi^*(L_b) \rightleftarrows$ ICT transition could be responsible for, or at least contribute to, the eventual electronic deactivation of the ICT to the S_0 state, as pointed out in our earlier publication on DMAde in water.[48] (iii) Additional decay channels for the ICT state in water might be opened up through hydrogen bonds with the solvent.

In the traditional picture for dual fluorescence from an ICT, which has been put forward especially for the prototypical DMABN molecule,[47] the mechanism is assumed to involve an electron transfer from the p-orbital of the exocyclic amino N atom into the π ring system starting in the planar configuration and follow a 90° rotation of the $-N(CH_3)_2$ group with respect to the ring. In particular, the excited-state dipole moment of the proposed twisted ICT (TICT) state was found to be an order of magnitude higher than that for the ground state. Moreover, time-resolved fluorescence measurements in the normal (LE state) and the anomalous (ICT state) emission bands of DMABN demonstrated a clear precursor−successor relationship between those states.[60] More recently, the visible fluorescence was found to occur with a time delay of ∼4 ps in acetonitrile at room temperature, which is exactly the decay time of the UV fluorescence.[61] Thus, although the TICT picture has been disputed in favor of alternative configurations (e.g., WICT, RICT, or PICT),[61] the basic ICT mechanism is widely accepted.

DMAde lacks the push−pull electronic structure of DMABN that is usually thought to facilitate an ICT,[47] but there are several other such cases known in the literature.[62] It is important that the fluorescence−time profiles of DMAde did not show major dependences on λ_{pump}, which one would expect by the influence of a potential energy barrier along the ICT reaction coordinate. Small variations seem to arise only due to the changes of the initially excited electronic states with λ_{pump} and in different solvents. Therefore, the ultrafast excited-state transformation to the ICT state in DMAde appears to take place through a CI and without any sizable activation energy. As in DMABN, the $\sigma_N\pi^*$ electronic configuration of a perpendicular (90° twist) TICT state would make fluorescence from that state forbidden, but additional configurational changes are likely to occur as well. Clearly, high-level ab initio calculations on DMAde would be of great interest to elucidate the unique electronic features and dynamics of this interesting nucleobase derivative compared to its parent compound Ade.

5. Conclusions

In this paper, we presented a comprehensive femtosecond time-resolved study of the dual fluorescence of DMAde in two different solvents, water and dioxane. The fluorescence was monitored at a series of wavelengths over the range of $290 \leq \lambda_{fl} \leq 650$ nm. Identical time constants were found following excitation just above the electronic origin ($\lambda_{pump} = 294$ nm) and at much shorter wavelengths, where excess energies of up to ∼5400 cm^{-1} ($\lambda_{pump} = 258$ nm) were deposited in the molecules.

The observed dynamics could be described with five well-defined time constants, ranging from sub-100 fs to 1.4 ns, each one corresponding to a distinctive molecular process.

Building on the information on the excited-state structure for the parent molecule 9H-Ade, the experimental data for DMAde were interpreted using a modified four-state model. Accordingly, the excited wavepacket leaves the FC region on the optically bright $\pi\pi^*(L_a)$ PEHS within ≤0.1 ps ($\tau_{1,w}$) to <0.3 ps ($\tau_{1,d}$) by following the steep gradient of the PEHS toward a local minimum of the $\pi\pi^*(L_a)$ state. As in 9H-Ade, the direct MEP leads to a $\pi\pi^*/S_0$ CI involving a biradical electronic structure and a large-amplitude puckering motion of the C^2H group. This main electronic deactivation pathway seems to be responsible for the measured ∼0.52−0.63 ps lifetimes ($\tau_{2,w}$, $\tau_{2,d}$). En route along the MEP, parts of the wavepackets are trapped and transform to the $\pi\pi^*(L_b)$ and/or $n\pi^*$ states, which appear to have lifetimes between 1.5 ($\tau_{3,w}$, $\tau_{3,d}$) and 10.9 ps ($\tau_{4,d}$).

Long-wavelength fluorescence was observed immediately after the pump pulse, consistent with a prompt population transfer from the optically bright to the ICT state, but such an

LE → ICT transition may be masked by the intense broad tail of the strong emission from the bright $\pi\pi^*(L_a)$ state. In any case, however, the distinctive emission band attributed to the ICT state is clearly developed after no less than 4−5 ps. The virtual absence of a dependence on λ_{pump} supports a practically barrierless population pathway. The much shorter fluorescence lifetime of the ICT state in water ($\tau_{5,w} \approx 62$ ps) than that in dioxane ($\tau_{5,d} \approx 1400$ ps) suggests that its eventual return mechanism to the S_0 is strongly affected by the solvent.

Complementary high-level ab inito calculations on DMAde are underway to shed further light on the proposed radiationless intramolecular deactivation pathways.

Acknowledgment. The financial support of this work by the Deutsche Forschungsgemeinschaft and the Fonds der Chemischen Industrie is gratefully acknowledged.

References and Notes

(1) Crespo-Hernandez, C. E.; Cohen, B.; Hare, P. M.; Kohler, B. *Chem. Rev.* **2004**, *104*, 1977.
(2) Pecourt, J.-M.; Peon, J.; Kohler, B. *J. Am. Chem. Soc.* **2000**, *122*, 9348.
(3) Pecourt, J.-M.; Peon, J.; Kohler, B. *J. Am. Chem. Soc.* **2001**, *123*, 10370.
(4) Peon, J.; Zewail, A. H. *Chem. Phys. Lett.* **2001**, *348*, 255.
(5) Cohen, B.; Hare, P. M.; Kohler, B. *J. Am. Chem. Soc.* **2003**, *125*, 13594.
(6) Onidas, D.; Markovitsi, D.; Marguet, S.; Gustavsson, T. *J. Phys. Chem. B* **2002**, *106*, 11367.
(7) Gustavsson, T.; Sharonov, A.; Onidas, D.; Markovitsi, D. *Chem. Phys. Lett.* **2002**, *356*, 49.
(8) Pancur, T.; Schwalb, N. K.; Renth, F.; Temps, F. *Chem. Phys.* **2005**, *313*, 199.
(9) Kwok, W.-M.; Ma, C.; Phillips, D. L. *J. Am. Chem. Soc.* **2006**, *128*, 11894.
(10) Kim, N. J.; Jeong, G.; Kim, Y. S.; Sung, J.; Kim, S. K.; Park, Y. D. *J. Chem. Phys.* **2000**, *113*, 10051.
(11) Lührs, D. C.; Viallon, J.; Fischer, I. *Phys. Chem. Chem. Phys.* **2001**, *3*, 1827.
(12) Plützer, C.; Nir, E.; de Vries, M. S.; Kleinermanns, K. *Phys. Chem. Chem. Phys.* **2001**, *3*, 5466.
(13) Nir, E.; Plützer, C.; Kleinermanns, K.; de Vries, M. *Eur. Phys. J. D* **2002**, *2002*, 317.
(14) Plützer, C.; Kleinermanns, K. *Phys. Chem. Chem. Phys.* **2002**, *4*, 4877.
(15) Kim, N. J.; Kang, H.; Park, Y. D.; Kim, S. K. *Phys. Chem. Chem. Phys.* **2004**, *6*, 2802.
(16) Lee, Y.; Schmidt, M.; Kleinermanns, K.; Kim, B. *J. Phys. Chem. A* **2006**, *110*, 11819.
(17) Zierhut, M.; Roth, W.; Fischer, I. *Phys. Chem. Chem. Phys.* **2004**, *6*, 5178.
(18) Hünig, I.; Plützer, C.; Seefeld, K. A.; Löwenich, D.; Nispel, M.; Kleinermanns, K. *Chem. Phys. Chem.* **2004**, *5*, 1427.
(19) Nix, M. G. D.; Devine, A. L.; Cronin, B.; Ashfold, M. N. R. *J. Chem. Phys.* **2007**, *126*, 124312.
(20) Wells, K.; Roberts, G.; Stavros, V. *Chem. Phys. Lett.* **2007**, *446*, 20.
(21) Kang, H.; Lee, K. T.; Jung, B.; Ko, Y. J.; Kim, S. K. *J. Am. Chem. Soc.* **2002**, *124*, 12958.
(22) Kang, H.; Jung, B.; Kim, S. K. *J. Chem. Phys.* **2003**, *118*, 6717.
(23) Canuel, C.; Mons, M.; Piuzzi, F.; Tardivel, B.; Dimicoli, I.; Elhaninea, M. *J. Chem. Phys.* **2005**, *122*, 074316.
(24) Ritze, H.-H.; Lippert, H.; Samoylova, E.; Smith, V. R.; Hertel, I.; Radloff, W.; Schulz, T. *J. Chem. Phys.* **2005**, *122*, 224320.
(25) Ullrich, S.; Schulz, T.; Zgierski, M. Z.; Stolow, A. *J. Am. Chem. Soc.* **2004**, *126*, 2262.
(26) Satzger, H.; Townsend, D.; Stolow, A. *Chem. Phys. Lett.* **2006**, *430*, 144.
(27) Satzger, H.; Townsend, D.; Zgierski, M. Z.; Patchkovskii, S.; Ullrich, S.; Stolow, A. *Proc. Natl. Acad. Sci. U.S.A.* **2006**, *103*, 10196.
(28) Sobolewski, A. L.; Domcke, W. *Eur. Phys. J. D* **2002**, *20*, 369.
(29) Perun, S.; Sobolewski, A. L.; Domcke, W. *Chem. Phys.* **2005**, *313*, 107.
(30) Perun, S.; Sobolewski, A. L.; Domcke, W. *J. Am. Chem. Soc.* **2005**, *127*, 6257.
(31) Marian, C. M. *J. Chem. Phys.* **2005**, *122*, 104314.
(32) Matsika, S. *J. Phys. Chem. A* **2005**, *109*, 7358.
(33) Nielsen, S. B.; Solling, T. I. *Chem. Phys. Chem.* **2005**, *6*, 1276.
(34) Chen, H.; Li, S. *J. Phys. Chem. A* **2005**, *109*, 8443.
(35) Blancafort, L. *J. Am. Chem. Soc.* **2006**, *128*, 210.
(36) Serrano-Andrés, L.; Merchán, M.; Borin, A. C. *Chem.—Eur. J.* **2006**, *12*, 6559.
(37) Marian, C. M.; Kleinschmidt, M.; Tatchen, *J. Chem. Phys.* **2008**, *347*, 346.
(38) Barbatti, M.; Lischka, H. *J. Am. Chem. Soc.* **2008**, *130*, 6831.
(39) Ward, D. C.; Reich, E.; Stryer, L. *J. Biol. Chem.* **1969**, *244*, 1228.
(40) Jean, J. M.; Hall, K. B. *Biochemistry* **2004**, *43*, 10277.
(41) Somsen, O. J. G.; Hoek, V. A.; Amerongen, H. *Chem. Phys. Lett.* **2005**, *402*, 61.
(42) Bonnist, E. Y. M.; Jones, A. C. *Chem. Phys. Chem.* **2008**, *9*, 1121.
(43) Serrano-Andrés, L.; Merchán, M.; Borin, A. C. *Proc. Natl. Acad. Sci. U.S.A.* **2006**, *103*, 8691.
(44) Albinsson, B. *J. Am. Chem. Soc.* **1997**, *119*, 6369.
(45) Andreásson, J.; Holmén, A.; Albinsson, B. *J. Phys. Chem. B* **1999**, *103*, 9782.
(46) Parusel, A. B. J.; Rettig, W.; Rotkiewicz, K. *J. Phys. Chem. A* **2002**, *106*, 2293.
(47) Grabowski, Z. R.; Rotkiewicz, K.; Rettig, W. *Chem. Rev.* **2003**, *103*, 3899.
(48) Schwalb, N. K.; Temps, F. *Phys. Chem. Chem. Phys.* **2006**, *8*, 5229.
(49) Wilhelm, T.; Piel, J.; Riedle, E. *Opt. Lett.* **1997**, *22*, 1494.
(50) Zhao, L.; Pérez Lustres, J. L.; Farztdinov, V.; Ernsting, N. P. *Phys. Chem. Chem. Phys.* **2005**, *7*, 1716.
(51) *Mathematica*, Version 6.0; Wolfram Research, Inc.: Champaign, IL, 2007.
(52) Maroncelli, M.; Fleming, G. R. *J. Chem. Phys.* **1987**, *86*, 6221.
(53) Eilers-König, N.; Kühne, T.; Schwarzer, D.; Vöhringer, P.; Schroeder, J. *Chem. Phys. Lett.* **1996**, *253*, 69.
(54) Pal, S. K.; Peon, J.; Zewail, A. H. *Chem. Phys. Lett.* **2002**, *363*, 57.
(55) Cohen, B.; Crespo-Hernández, C. E.; Kohler, B. *Faraday Discuss.* **2004**, *127*, 137.
(56) The nominal lifetimes from the fits at $\lambda_{fl} = 300$ and 310 nm were as short as $\tau_1 = 0.054(2)$ ps.
(57) Pancur, T. Investigation of the Isomerization Dynamics of Azobenzenes and the Radiationless Deactivation of Nucleobases Using Femtosecond Fluorescence Spectroscopy. Ph.D. Thesis, Christian-Albrechts-University, Kiel, Germany, 2004.
(58) Zgierski, M. Z.; Patchkovskii, S.; Lim, E. C. *Can. J. Chem.* **2007**, *85*, 124.
(59) Bisgaard, C. Z.; Satzger, H.; Ullrich, S.; Stolow, A. *Chem. Phys. Chem.* **2009**, *10*, 101.
(60) Changenet, P.; Plaza, P.; Martin, M. M.; Meyer, Y. H. *J. Phys. Chem.* **1997**, *101*, 8186.
(61) Druzhinin, S. I.; Ernsting, N. P.; Kovalenko, S. A.; Pérez Lustres, L.; Senyushkina, T. A.; Zachariasse, K. *J. Phys. Chem. A* **2006**, *110*, 2955.
(62) Yoshihara, T.; Druzhinin, S. I.; Zachariasse, K. A. *J. Am. Chem. Soc.* **2004**, *126*, 8535.

JP9021773